



Universal Electromotive Force Induced by Domain Wall Motion

Shengyuan A. Yang, Geoffrey S. D. Beach, Carl Knutson, Di Xiao, Qian Niu, Maxim Tsoi, and James L. Erskine

Department of Physics, The University of Texas, Austin, Texas, 78712-0264, USA

(Received 29 July 2008; published 9 February 2009)

The electromotive force induced by a moving magnetic domain wall in a nanostrip has been calculated theoretically and detected experimentally. It is found that the emf depends only on the domain wall transformation frequency through a universal Josephson type relation, which is closely related to the topological nature of the domain wall. Our experimental measurements confirm the theoretical prediction.

DOI: 10.1103/PhysRevLett.102.067201

PACS numbers: 75.75.+a, 72.25.Ba, 75.47.-m, 75.60.Ch

The interplay between charge transport and spin dynamics is a central theme of spintronics research. It is now well established that an electric current can drive magnetic domain wall (DW) motion via coupling between conduction electrons and local magnetic moments [1–5]. The reverse of this effect, i.e., an emf induced by a DW moving through a stationary electron gas, has also been predicted [6]. Recently there has been renewed interest in this effect [7–9], and its connection with Berry phase [10] has highlighted important topological aspects. However, prior theoretical work on DW-induced emf has only treated simple 1D walls, rather than more realistic 2D wall geometries [11,12], and no experimental detection has yet been reported. In this Letter, we formalize Berger’s original result, generalize it to 2D DWs, and report the first experimental evidence for DW-driven emf.

To describe electron dynamics in ferromagnetic metals we adopt the *s-d* model, in which conduction electrons interact with local magnetic moments through an exchange coupling $H_{sd} = -J\hat{n}(\mathbf{r}, t) \cdot \boldsymbol{\sigma}$. The unit vector \hat{n} denotes the local spin direction, $\boldsymbol{\sigma}$ is the itinerant electron spin, and J is the coupling strength. For typical ferromagnetic metals (Co, Fe, Ni and their alloys), *s-d* coupling is strong ($J \sim 1$ eV), and the conduction electron spin follows the local spin direction during its motion. Then the spatial variation of the local spin texture gives rise to the well-known Berry curvature field $\mathbf{C}(\mathbf{r}, t) = (1/2) \sin\theta(\nabla\theta \times \nabla\phi)$, where (θ, ϕ) are the spherical angles specifying the direction of \hat{n} . The \mathbf{C} -field acts on the electrons as an effective magnetic field whose flux enclosed by a loop gives the Berry phase of the spin-1/2 particle that moves around the loop. This is analogous to the Aharonov-Bohm phase acquired by a charged particle moving around a magnetic flux. Furthermore, in analogy with the electric field that arises from motion of a magnetic field, the \mathbf{C} -field of a moving spin texture also generates an effective electric field $\mathbf{D}(\mathbf{r}, t) = (1/2) \sin\theta(\partial_t\phi\nabla\theta - \partial_t\theta\nabla\phi)$ [13]. These fields can be derived directly from the semiclassical equation of motion for an electron wave packet [14], where the force on the conduction electrons from a moving spin texture can be shown to be $\mathbf{F} = -\hbar(\dot{\mathbf{r}} \times \mathbf{C} + \mathbf{D})$. This \mathbf{D} -field is the origin of the emf generated by a moving DW.

In this work, we consider a DW confined in a ferromagnetic nanostrip. Depending on the strip size, the static configuration of the DW can be either a (1D) transverse DW or a vortex DW [11]. Berger’s phenomenological approach [6] predicted a voltage $V_x = (\hbar/e)d\psi/dt$ generated across a transverse DW-driven by a field beyond the Walker precessional threshold [15], which was termed ferro-Josephson effect due to its resemblance to the Josephson relation in superconductivity. Here subscript *x* labels the longitudinal direction of the nanostrip, \hbar is the reduced Planck constant, $-e$ is the electron charge, and ψ is the tilt angle of the rigidly precessing DW plane. Berger’s prediction follows rigorously from our Berry phase approach. The \mathbf{D} -field of a moving transverse wall, integrated along the direction of its motion, exactly reproduces Berger’s result and is independent of the detailed form of the wall.

The large magnetostatic energy associated with rigid wall plane canting causes 1D DW models to fail at relatively low fields [16,17]. In nanostrips (width w , thickness t , where $w \gg t$), well before the 1D Walker field is reached [16], a vortex core periodically nucleates in a DW at the wire edge and slowly travels across the wire [18]. Therefore the dynamic wall-structure evolution, via gyrotropic vortex motion, requires a fully 2D treatment of the vortex structure. A vortex DW is characterized by a small core region with radius a (\sim several nm), in which \hat{n} points out of the 2D plane. The Berry curvature field \mathbf{C} is nonzero only inside the vortex core and its integral over the 2D plane gives the topologically invariant Skyrmin charge associated with the vortex [19], i.e., $\int \mathbf{C} d^2r = pq\pi\hat{e}_z$, which is independent of the detailed profile of the vortex. Here $p, q = \pm 1$ are the polarization and vorticity of the vortex, respectively.

We calculate the emf induced by the motion of a 2D vortex DW by solving the Poisson equation $\nabla^2 V = (\hbar/e)\nabla \cdot \mathbf{D}$ with Neumann boundary conditions (no current leaving the sample). We find that the \mathbf{D} -field is that of an electric dipole \mathbf{P} located within the vortex core,

$$\mathbf{P} = \varepsilon_0 \frac{\hbar}{e} \int \mathbf{D} d^2r = \varepsilon_0 \frac{\hbar}{e} pq\pi\hat{e}_z \times \mathbf{v}, \quad (1)$$

where we use $\mathbf{D} = \mathbf{C} \times \mathbf{v}$ for rigid DW motion with \mathbf{v} being the velocity of the vortex core. Since $a \ll w$, \mathbf{P} can be treated as a point dipole. By the method of image charge, we find that the longitudinal voltage drop along the direction of the DW propagation is

$$V_x = \pi \frac{\hbar}{e} \frac{|v_y|}{w}. \quad (2)$$

Transverse vortex motion results from the Magnus force [20]. At low fields, this force is balanced by the confining potential of the wire, and $v_y = 0$. Above the breakdown transition, the Magnus force overcomes the confining potential and the vortex core within a DW is driven to the wire edge. There, it annihilates and a new vortex with opposite polarization is emitted, and is driven to the other edge [21,22]. Since both p and v_y change sign at the edge while q is kept, the sign of the product pqv_y is conserved during the periodic process, leading to a nonzero dc voltage across the wall whose polarity is unchanged for a unidirectional DW propagation (along the x direction). Its time average depends only on the frequency f of transverse motion, i.e. $\bar{V}_x = 2\pi(\hbar/e)f$. This result, together with the result for 1D DW, reveal a universal Josephson type relation with the Josephson frequency being the frequency of DW transformation. Moreover, our derivation demonstrates clearly that this remarkable result is intimately related to the topological nature of DW.

If the DW is driven by an applied magnetic field H , it has been shown that this frequency is the Larmor frequency, $2\pi f = \gamma H$ [22,23], where γ is the gyromagnetic ratio. Then the average voltage is linear in the applied field, with $\bar{V}_x/H = (\hbar/e)\gamma \approx 11.6$ nV/Oe. Accounting for spin minority carriers amounts to multiplying the predicted

voltage by the spin-polarization factor P . Additional voltages from nonadiabatic or dissipative effects, estimated through force balance considerations [8,24], are found to be at least 10 times smaller than the adiabatic contribution above breakdown, though they are the only contribution below breakdown.

We have detected the longitudinal voltage generated by the motion of a single DW using the technique outlined in Fig. 1. The DW was confined within a Ni₈₀Fe₂₀ (Permalloy, Py) nanowire, 500 nm wide, 20 nm thick, and 35 μm long, that was joined to a large Py “injection pad” at one end and tapered to a point at the other. A field applied antiparallel to the wire magnetization (which lies along its axis) reverses the magnetically-soft pad and generates a DW at the pad-wire junction which is of vortex type according to the phase diagram [11]. If the field exceeds the DW injection field H_{inj} , the DW enters and traverses the wire from left to right. A nonmagnetic Pt bridge connected the pointed end of the wire to a second large Py pad. Electrical contacts made to the pads allowed the voltage across the wire to be measured as the DW traveled along it.

A high-frequency (~ 320 kHz) square-wave drive-field of amplitude H_d was used to repeatedly inject and drive DWs along the wire. The drive-field half-period $T_{1/2}$ exceeded the DW transit time τ_{DW} [see Fig. 1(e)], allowing each DW to reach the end of the wire before a new wall was injected. The high slew-rate fields used to inject and drive DWs generated large inductive voltages (tens of mV) in the measurement circuit. To extract the comparatively small voltage induced by DW motion (~ 100 nV), a modulation scheme was employed. In this approach, a secondary magnet was used to apply two additional fields: a 317 Hz square-wave modulation field (amplitude $H_m = 11$ Oe)

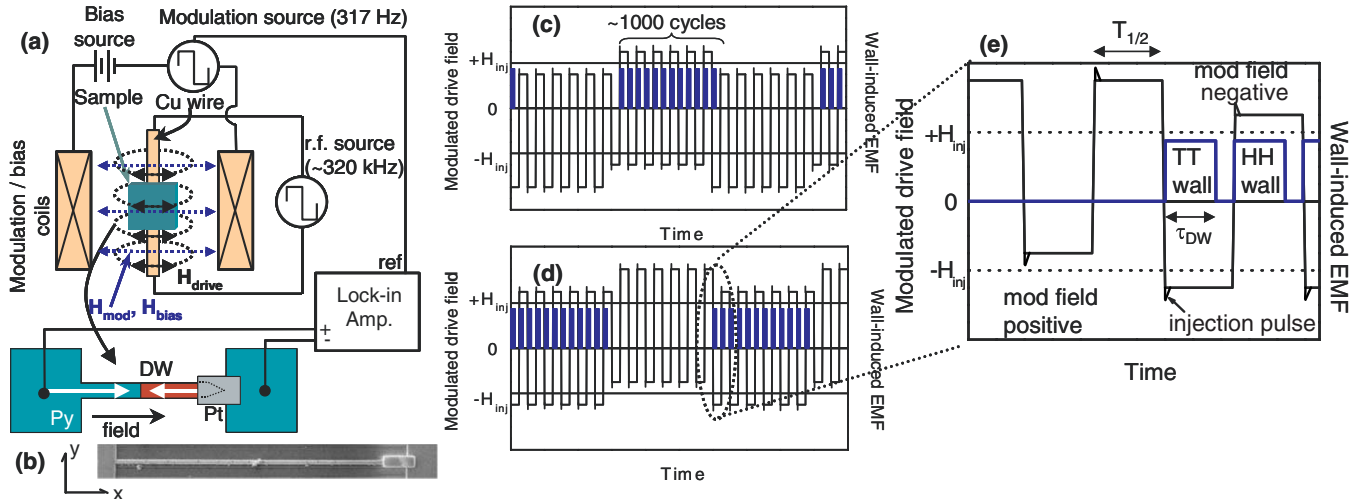


FIG. 1 (color online). Experiment schematic. (a) Drive, modulation, and bias field configuration with respect to sample. (b) Scanning electron micrograph of nanowire device. (c),(d) Total field waveform for two bias field levels. Injection field H_{inj} indicated by horizontal lines. Black solid lines indicate field waveform; blue indicates voltage signal expected from DW moving along nanowire. (e) Detail of several drive-field cycles immediately before and after a step in the modulation field. Before the step, the nanowire is saturated and no DWs travel along it. After the step, each drive-field half-cycle (duration $T_{1/2}$) injects a DW that moves along the wire, generating a voltage until it reaches the end of the wire after a time τ_{DW} .

plus a dc bias field H_{dc} which can be tuned. These two fields were used to modulate the probability that DWs were injected by H_d . Their combined effect is like a “switch” which can periodically turn the DW voltage signal “on” and “off.”

The sum of these fields as a function of time is shown schematically in Fig. 1 for two values of H_{dc} ($= \pm H_m$). For the negatively biased ($H_{dc} < 0$) waveform of Fig. 1(c), a DW is injected and driven across the wire at the beginning of the negative phase of the modulation cycle. Because the positive-going drive-field steps are biased below the DW injection threshold, no further DW motion occurs within the wire until the positive phase of the modulation cycle. During that phase, H_{total} oscillates symmetrically about zero and DWs, alternately head-to-head and tail-to-tail, are repeatedly injected and driven to the end of the nanowire. Each DW travels in the same direction, leading to a rapid sequence of voltage pulses with the same polarity and nonzero dc level. The voltage across the nanowire was measured using a lock-in amplifier phase-locked to the 317 Hz modulation field source [Fig. 1(a)], thereby rejecting rf inductive pickup at the drive frequency. The in-phase (real) lock-in voltage component, V_L , is proportional to the difference in the average wall-induced voltage between the positive and negative phases of the modulation field cycle.

The system has a rather high injection threshold $H_{inj} \approx 37$ Oe. In order to study the emf for a driving field with $H_d < H_{inj}$, we add to the high-frequency drive-field waveform a short “injection pulse” (45 Oe peak, ~ 60 ns FWHM) [16] preceding each half-cycle [see Fig. 1(e)]. Each pulse briefly exceeded H_{inj} , injecting a DW which then propagated under a lower field H_d . This permitted the study of walls driven by a range of fields H_d , while maintaining identical injection characteristics. DW injection and propagation were probed using high-bandwidth scanning Kerr polarimetry [16]. The probability of wall injection, P_{inj} , as a function of H_{dc} was detected (with H_m set to zero here). At $H_{dc} = 0$, each injection pulse exceeds H_{inj} , and $P_{inj} = 1$. When a bias $|H_{dc}| > 8$ Oe is applied, P_{inj} drops as either the positive or negative-going injection pulse is shifted below the (full) injection threshold. When the injection pulse is omitted, at least one side of the drive waveform is always below the DW injection threshold for any H_{dc} , so $P_{inj} = 0$ and no DW-induced voltage is expected.

The modulation field $H_m = 11$ Oe was used to toggle P_{inj} , thereby modulating the DW-induced voltage. The detected lock-in voltage V_L should be proportional to the difference in P_{inj} between the positive and negative phases of the modulation cycle, weighted by the average DW-induced voltage in each of those phases. The lock-in voltage V_L at $H_d = 20$ Oe is shown in Fig. 2(a) as a function of the dc bias field H_{dc} . We observe that it is more complex than that expected from motion of a single DW along the nanowire. The large offset voltage is due primarily to inductive pickup of the modulation field by the

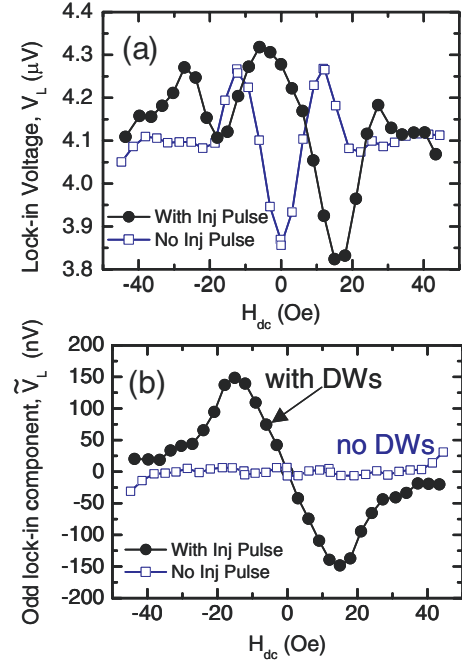


FIG. 2 (color online). (a) Lock-in voltage versus H_{dc} for the drive-field waveforms with $H_d = 20$ Oe with/and without injection pulse. (b) Odd components of the curves in (a).

measurement loop, and it scales linearly with the modulation field frequency and amplitude. The dependence of V_L on H_{dc} , particularly when injection pulses are omitted from the drive-field waveform, points to additional sources of modulated voltage. The contact or injection pads are magnetic, and likely contribute in nontrivial ways to the measured signal. For example, DW motion within the pads could contribute a net emf, and stray magnetostatic fields could lead to a bias field-dependant flux through the measurement loop.

To discriminate between voltage generated by DW motion along the nanowire, and other parasitic contributions, we exploit the fact that unidirectional DW motion generates a voltage with definite polarity that does not depend on the sign of the total driving field [cf. discussion following Eq. (2)]. Hence any DW-induced contribution to V_L must

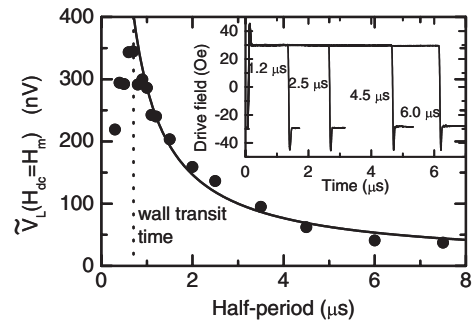


FIG. 3. Odd-symmetry component of lock-in voltage at $H_{dc} = H_m$ for drive-field waveforms of varying half-period $T_{1/2}$ (half-cycles shown in inset). Solid line is fit to $1/T_{1/2}$.

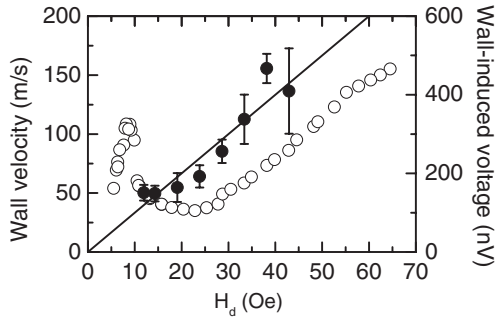


FIG. 4. Measured wall velocity (open symbols) and wall-induced voltage (solid symbols) versus drive-field. Solid line is fit with slope 10 nV/Oe.

be odd in H_{dc} : comparing Figs. 1(c) and 1(d), the modulated DW voltage has the same amplitude for $\pm H_{dc}$, but it is in-phase with the modulation field for negative bias, and out of phase for positive bias. This phase difference manifests as a sign change in the DW contribution to V_L .

Figure 2(b) shows the odd component \tilde{V}_L of the data in Fig. 2(a). When the drive-field includes injection pulses, V_L contains an odd component that closely follows the modulated DW injection probability measured experimentally. When injection pulses are omitted from the drive waveform, and hence DW motion does not occur within the nanowire, there is no voltage contribution with this symmetry. Based on its symmetry and its correlation with P_{inj} , we interpret \tilde{V}_L as arising from DW motion along the nanowire.

This identification is supported by additional systematic tests that correlate the magnitude of \tilde{V}_L with the motion of the DW. The contribution to \tilde{V}_L by DWs traversing the nanowire is proportional to the ratio $\tau_{DW}/T_{1/2}$ [cf. Fig. 1(e)]. τ_{DW} will be the same for each drive-field half-cycle if we set $H_{dc} = H_m$ such that the drive-field waveform has zero offset during the on phase of the modulation cycle, and each injected wall is driven by a field of amplitude $\pm H_d$ [cf. Figs. 1(c) and 1(d)]. Figure 3 shows \tilde{V}_L measured at $H_{dc} = H_m$ for a series of drive-field waveforms with varying period. \tilde{V}_L varies inversely with $T_{1/2}$, except for $T_{1/2} < 0.7 \mu\text{s}$, where \tilde{V}_L drops precipitously. This crossover time corresponds to the independently measured wall transit time τ_{DW} . At $T_{1/2} = \tau_{DW}$, DWs generate voltage over the full duration of each drive-field cycle. For $T_{1/2} < \tau_{DW}$, a DW injected into a uniform wire generates voltage during the first drive-field half-period, but before it reaches the end of the wire, H_d changes polarity. A new DW is injected and moves forward while the initial wall moves back, giving zero net voltage. Averaged over a full drive-field cycle, \tilde{V}_L should drop, consistent with Fig. 3.

$\tilde{V}_L(H_{dc})$ was also measured for a series of drive-field waveforms with the same injection pulse, but with varying H_d . The curves followed Fig. 2(b), varying only in amplitude. At $H_{dc} = H_m$, \tilde{V}_L is proportional to the voltage V_{DW} generated by a DW driven by a field $|H_d|$, i.e., $V_{DW}(H_d) = C(T_{1/2}/\tau_{DW})\tilde{V}_L[H_{dc} = H_m]$, where $C^{-1} = 4/\pi$ is the

weight of the fundamental Fourier component of a square-wave. The average DW velocity, shown in Fig. 4, was independently-measured, yielding τ_{DW} . The dependence of V_{DW} on H_d is shown in Fig. 4 [25]. V_{DW} varies in proportion to field, with a slope of ~ 10 nV/Oe. This is close to the predicted slope $\gamma\hbar/e = 11.6$ nV/Oe, and suggests a spin-polarization $P \sim 0.85$, somewhat higher than expected but within reasonable experimental bounds.

In summary, we have developed a general theory to calculate the emf generated by the motion of an arbitrary spin texture and obtained a universal ferro-Josephson relation for a DW moving in a nanostrip. The theory yields a universal result $V_x/H = 11.6$ nV/Oe for a field-driven DW, independent of the details of its internal structure. We have detected experimentally the voltage generated during the motion of a single domain wall over a range of driving field and find a result that agrees well with this prediction.

The authors thank C. Xu, W. Li, C.-P. Chuu, W. Yao, D. Clougherty, and S. Zhang for valuable discussions. S. Y., G. B., C. K., M. T., and J. E. were supported by NSF DMR-0404252, DX was supported by NSF DMR-0606485, G. B. and J. E. by the Welch Foundation, and Q. N. by DOE (DE-FG03-02ER45958).

- [1] P. P. Freitas and L. Berger, J. Appl. Phys. **57**, 1266 (1985).
- [2] A. Yamaguchi *et al.*, Phys. Rev. Lett. **92**, 077205 (2004).
- [3] M. Kläui *et al.*, Phys. Rev. Lett. **95**, 026601 (2005).
- [4] G. S. D. Beach *et al.*, Phys. Rev. Lett. **97**, 057203 (2006).
- [5] M. Hayashi *et al.*, Phys. Rev. Lett. **96**, 197207 (2006).
- [6] L. Berger, Phys. Rev. B **33**, 1572 (1986).
- [7] S. E. Barnes *et al.*, Appl. Phys. Lett. **89**, 122507 (2006); S. E. Barnes and S. Maekawa, Phys. Rev. Lett. **98**, 246601 (2007).
- [8] R. A. Duine, Phys. Rev. B **77**, 014409 (2008).
- [9] W. M. Saslow, Phys. Rev. B **76**, 184434 (2007).
- [10] M. V. Berry, Proc. R. Soc. A **392**, 45 (1984).
- [11] R. D. McMichael and M. J. Donahue, IEEE Trans. Magn. **33**, 4167 (1997).
- [12] M. Kläui *et al.*, Appl. Phys. Lett. **85**, 5637 (2004).
- [13] G. E. Volovik, J. Phys. C **20**, L83 (1987).
- [14] G. Sundaram and Q. Niu, Phys. Rev. B **59**, 14915 (1999).
- [15] N. L. Schryer and L. R. Walker, J. Appl. Phys. **45**, 5406 (1974).
- [16] G. S. D. Beach *et al.*, Nature Mater. **4**, 741 (2005).
- [17] G. S. D. Beach, M. Tsoi, and J. L. Erskine, J. Magn. Magn. Mater. **320**, 1272 (2008).
- [18] Y. Nakatani *et al.*, Nature Mater. **2**, 521 (2003).
- [19] A. A. Belavin and A. M. Polyakov, Pis'ma Zh. Eksp. Teor. Fiz. **22**, 503 (1975) [JETP Lett. **22**, 245 (1975)].
- [20] J. Shibata *et al.*, Phys. Rev. B **73**, 020403(R) (2006).
- [21] J. He *et al.*, Phys. Rev. B **73**, 184408 (2006).
- [22] J.-Y. Lee *et al.*, Phys. Rev. B **76**, 184408 (2007).
- [23] M. Hayashi *et al.*, Nature Phys. **3**, 21 (2007).
- [24] L. Berger, J. Appl. Phys. **55**, 1954 (1984).
- [25] Voltage generated during the injection pulse adds to the calculated $V_{DW}(H_d)$, and has not been corrected for.